Center for Turbulence Research
Proceedings of the Summer Program 2010

A multi-Gaussian quadrature method of moments for gas-particle flows in a LES framework

By C. Chalons†, R. O. Fox‡ AND M. Massot†

The purpose of the present contribution is to introduce a new high-order moment formalism for particle/droplet trajectory crossing (PTC) in the framework of large-eddy simulation (LES) of gas-particle flows. Thus far, the ability to treat PTC has been examined by several investigators for direct numerical simulations (DNS) using quadrature-based moment methods based on a sum of Dirac delta functions (Yuan & Fox (2010), Kah et al. (2010)). However, for LES, such methods require too many moments in order to capture both the effect of subgrid-scale turbulence on the disperse phase as well as PTC due to large-scale eddies in a Eulerian mesoscopic framework. The challenge is thus twofold: first, to propose a new generation of quadrature with less singular behavior as well as associated proper mathematical properties and related algorithms, and second to limit the number of moments used for applicability in multi-dimensional configurations without losing accuracy in the representation of spatial fluxes.

1. Introduction

The physics of particles and droplets in a carrier gaseous flow field are described in many applications (fluidized beds, spray dynamics, alumina particles in rocket boosters, ...) by a number density function (NDF) satisfying a kinetic equation. Solving such a kinetic equation relies on either a sample of discrete numerical parcels of particles through a Lagrangian–Monte-Carlo approach or on a moment approach resulting in a Eulerian system of conservation laws on velocity moments eventually conditioned on size. In the latter case investigated in the present contribution, the main difficulty for particle flows with high Knudsen numbers (i.e., weakly collisional flows), where the velocity distribution can be very far from equilibrium, is the closure of the convective transport at the macroscopic level. One way to proceed is to use quadrature-based moment methods where the higher-order moments required for closure are evaluated from the lower-order transported moments using multi-dimensional quadratures in the form of a sum of Dirac delta functions in velocity phase space (see Yuan & Fox (2010) and the references therein for a series of advances within this framework). Such an approach also allows for a well-behaved kinetic numerical scheme in the spirit of Bouchut et al. (2003) (from de Chaisemartin (2009) to Kah et al. (2010), Fréret et al. (2010), Yuan & Fox (2010)) where the fluxes in a cell-centered finite-volume formulation are directly evaluated from the knowledge of the quadrature abscissas and weights with guaranteed realizability conditions. Such a quadrature approach and the related numerical methods have been shown to be able to capture PTC in a DNS context, where the distribution

† Laboratoire EM2C - UPR CNRS 288, Ecole Centrale Paris, Grande voie des vignes, 92295 Chatenay Malabry, France
‡ Iowa State University, Department of Chemical and Biological Engineering, Ames, IA 50011-2230 USA

in the exact kinetic equation remains at all times in the form of a sum of Dirac delta functions, and can be extended to high-order numerical schemes, see Vikas et al. (2010).

In a LES framework, the effect of the subgrid scales (SGS) of the turbulent gaseous flow field can lead to dispersion in velocity phase space for the particles, which can be described by Fokker-Planck-like models introduced in Reeks (1991). Nevertheless, in a LES framework PTC still occurs for large enough Stokes numbers in the high Knudsen number limit because the SGS dispersion is not strong enough to "randomize" the particle velocities resulting from free kinetic transport. However, capturing both PTC as well as velocity dispersion (caused by SGS agitation around the Dirac delta function representation of PTC) would require a large number of quadrature nodes using a delta function representation. Moreover, such quadrature-based methods result in entropic weakly hyperbolic systems of conservation laws and to the formation of δ-shock singularities, the mathematical structure of which is studied in Kah et al. (2010). The purpose of the present contribution is to introduce a novel quadrature-based moment approach for the resolution of the free-transport part of the filtered kinetic equation (i.e., PTC), which also allows us to naturally account for velocity dispersion. Note that since the free-transport term in the filtered kinetic equation has exactly the same form as in the original kinetic equation, see Zaichik et al. (2009), hereafter we do not make the distinction between the two forms. The proposed quadrature approach allows us both to limit the number of unknowns in multi-dimensional configurations, and to regularize the resulting system of conservation equations, while still being able to capture PTC and velocity dispersion in the LES framework.

We first introduce the new moment formalism, quadrature and numerical methods, using the NDF $f(t,x,v)$ in 1-D for the free-transport kinetic equation

$$\partial_t f + v\partial_x f = 0, \quad t>0,\, x\in\mathbb{R},\, v\in\mathbb{R}, \tag{1.1}$$

with initial condition $f(0,x,v) = f_0(x,v)$. The exact solution is given by $f(t,x,v) = f(0,x-vt,v) = f_0(x-vt,v)$. Then, in order to justify the advantages of such an approach in multi-dimensions, we switch to the 2-D case in velocity phase space with NDF $f(t,x,\mathrm{v})$ for $\mathrm{v}=(u,v)^t$, which is homogeneous in the y direction, and satisfies:

$$\partial_t f + u\partial_x f = 0, \quad t>0,\, x\in\mathbb{R},\, \mathrm{v}\in\mathbb{R}^2, \tag{1.2}$$

with initial condition $f(0,x,\mathrm{v}) = f_0(x,\mathrm{v})$. With a 2-D velocity phase space, we approximate the solution to f using a quadrature representation found from the bivariate moments. Finally, once the quadrature representation has been mathematically justified and the algorithms have been presented for 1-D and 2-D cases, we present numerical results for the Riemann problem in both cases, thus showing the potential of the approach as well as the smoothness of the solutions compared to the standard Dirac quadrature.

2. 1-D kinetic model, multi-Gaussian quadrature, and related algorithms

2.1. *1-D moment transport equations*

Defining the i-order moment $M_i(t,x) = \int_v f(t,x,v)v^i dv$, $i=0,\ldots,N$, $N\in\mathbb{N}$, the associated governing equations are easily obtained from (Eq. 1.1) after multiplication by v^i and integration over v: $\partial_t M_i + \partial_x M_{i+1} = 0$, $i\geq 0$. For simplicity, but without any loss of generality, we will focus our attention hereafter on the five-moment model and its

abstract form:

$$\left\{\begin{array}{l}\partial_t M_0+\partial_x M_1=0,\\ \partial_t M_1+\partial_x M_2=0,\\ \partial_t M_2+\partial_x M_3=0,\\ \partial_t M_3+\partial_x M_4=0,\\ \partial_t M_4+\partial_x \overline{M}_5=0.\end{array}\right. , \quad \partial_t \mathbf{M}+\partial_x \mathbf{F}(\mathbf{M})=0, \tag{2.1}$$

with $\mathbf{M}=(M_0,M_1,M_2,M_3,M_4)^t$ and $\mathbf{F}(\mathbf{M})=(M_1,M_2,M_3,M_4,\overline{M}_5)^t$. This model is closed provided that $\overline{M}_5$ is defined as a function of $\mathbf{M}$. Here we propose to define this function by representing f as a bi-Gaussian distribution function.

2.2. *1-D bi-Gaussian distribution*

The starting point to define the moment closure consists in representing the velocity distribution $f(t,x,v)$ by the sum of two Gaussian functions:

$$f^{\mathrm{G}}(t,x,v)=\frac{\rho_1(t,x)}{\sigma\sqrt{2\pi}}\exp\left(-\frac{(v-v_1(x,t))^2}{2\sigma^2}\right)+\frac{\rho_2(t,x)}{\sigma\sqrt{2\pi}}\exp\left(-\frac{(v-v_2(x,t))^2}{\sigma^2}\right), \tag{2.2}$$

where the weights $\rho_1(t,x)>0$, $\rho_2(t,x)>0$, the velocity abscissas $v_1(t,x)$, $v_2(t,x)$ and the common spread $\sigma\geq 0$ must be uniquely determined from the knowledge of $\mathbf{M}(x,t)$. Dropping the (x,t)-dependence to avoid cumbersome notation, the function f^{G} has exact moments M_i^{G} of orders $i=0,...,5$ given by

$$\left\{\begin{array}{l}M_0^{\mathrm{G}}=\rho_1+\rho_2,\\ M_1^{\mathrm{G}}=\rho_1 v_1+\rho_2 v_2,\\ M_2^{\mathrm{G}}=\rho_1(\sigma^2+v_1^2)+\rho_2(\sigma^2+v_2^2),\\ M_3^{\mathrm{G}}=\rho_1 v_1(3\sigma^2+v_1^2)+\rho_2 v_2(3\sigma^2+v_2^2),\\ M_4^{\mathrm{G}}=\rho_1 v_1^2(6\sigma^2+v_1^2)+\rho_2 v_2^2(6\sigma^2+v_2^2)+3\sigma^4(\rho_1+\rho_2),\\ M_5^{\mathrm{G}}=\rho_1 v_1^3(10\sigma^2+v_1^2)+\rho_2 v_2^3(10\sigma^2+v_2^2)+15\sigma^4(\rho_1 v_1+\rho_2 v_2).\end{array}\right.$$

The moment closure for (Eq. 2.1) then naturally consists in setting $\overline{M}_5=M_5^{\mathrm{G}}$ where the five unknowns ρ_1, ρ_2, v_1, v_2 and σ^2 are found by solving the nonlinear system $M_i=M_i^{\mathrm{G}}$, $i=0,\ldots,4$; which is clearly equivalent to solving the system

$$\left\{\begin{array}{l}M_0=\rho_1+\rho_2,\\ M_1=\rho_1 v_1+\rho_2 v_2,\\ M_2-\sigma^2 M_0=\rho_1 v_1^2+\rho_2 v_2^2,\\ M_3-3\sigma^2 M_1=\rho_1 v_1^3+\rho_2 v_2^3,\\ M_4-6\sigma^2 M_2+3\sigma^4 M_0=\rho_1 v_1^4+\rho_2 v_2^4.\end{array}\right. \tag{2.3}$$

It remains to prove that this system is well-posed in the following proposition.

PROPOSITION 1. *For $\mathbf{M}=(M_0,M_1,M_2,M_3,M_4)^t$ such that $M_0>0$, let us define*

$$e=\frac{M_0M_2-M_1^2}{M_0^2},\quad q=\frac{(M_3M_0^2-M_1^3)-3M_1(M_0M_2-M_1^2)}{M_0^3},$$

and

$$\eta=\frac{-3M_1^4+M_4M_0^3-4M_0^2M_1M_3+6M_0M_1^2M_2}{M_0^4}.$$

System (2.3) is well-defined on the phase space Ω given by

$$\Omega=\{\mathbf{M}=(M_0,M_1,M_2,M_3,M_4)^t, M_0>0, e>0, \eta>e^2+\frac{q^2}{e},\ \textit{and}\ \eta\leq 3e^2\ \textit{if}\ q=0\}.$$

Setting $\mathbf{U} = (\rho_1, \rho_2, \rho_1 v_1, \rho_2 v_2, \sigma)^t$, *the function* $\mathbf{U} = \mathbf{U}(\mathbf{M})$ *is one-to-one and onto as soon as* $v_1 \neq v_2$, *and for all* v_1 *and* v_2 *provided that we set* $\rho_1 = \rho_2$ *in the case* $v_1 = v_2$. *Moreover,* σ^2 *is given by the unique real root of the third-order polynomial*

$$\left\{ \begin{array}{l} \mathcal{P}(\sigma_0) = 2\sigma_0^3 + (\eta - 3e^2)\sigma_0 + q^2, \\ \sigma_0 = \sigma^2 - e. \end{array} \right.$$

Proof. We first set $\overline{\rho}_1 = \frac{\rho_1}{M_0}$, $\overline{\rho}_2 = \frac{\rho_2}{M_0}$, $\overline{v}_1 = v_1 - \frac{M_1}{M_0}$, $\overline{v}_2 = v_2 - \frac{M_1}{M_0}$, solving (Eq. 2.3) is equivalent to solving

$$\left\{ \begin{array}{l} 1 = \overline{\rho}_1 + \overline{\rho}_2, \\ 0 = \overline{\rho}_1 \overline{v}_1 + \overline{\rho}_2 \overline{v}_2, \\ e - \sigma^2 = \overline{\rho}_1 \overline{v}_1^2 + \overline{\rho}_2 \overline{v}_2^2, \\ q = \overline{\rho}_1 \overline{v}_1^3 + \overline{\rho}_2 \overline{v}_2^3, \\ \eta - 6\sigma^2 e + 3\sigma^4 = \overline{\rho}_1 \overline{v}_1^4 + \overline{\rho}_2 \overline{v}_2^4. \end{array} \right.$$

with $e = (M_0 M_2 - M_1^2)/M_0^2$, $q = ((M_3 M_0^2 - M_1^3) - 3M_1(M_0 M_2 - M_1^2))/M_0^3$, $\eta = (-3M_1^4 + M_4 M_0^3 - 4M_0^2 M_1 M_3 + 6M_0 M_1^2 M_2)/M_0^4$. Dropping the overlines for the sake of clarity, it is then a matter to uniquely solve the following nonlinear system in $(\rho_1, \rho_2, v_1, v_2, \sigma^2)$:

$$\left\{ \begin{array}{l} \rho_1 + \rho_2 = 1, \\ \rho_1 v_1 + \rho_2 v_2 = 0, \\ \rho_1 v_1^2 + \rho_2 v_2^2 = e - \sigma^2, \\ \rho_1 v_1^3 + \rho_2 v_2^3 = q, \\ \rho_1 v_1^4 + \rho_2 v_2^4 = \eta - 6\sigma^2 e + 3\sigma^4. \end{array} \right. \tag{2.4}$$

Provided $e \geq \sigma^2$, it is proved in Desjardins et al. (2008) that the first four equations allow us to find $(\rho_1, \rho_2, v_1, v_2)$. We will then focus on the last equation to find σ^2.

In the case $q = 0$, the second and fourth equations yield $\rho_1 v_1 (v_1^2 - v_2^2) = 0$, and $\rho_2 v_2 (v_1^2 - v_2^2) = 0$, which gives $v := v_1 = -v_2$. We then get $\rho_1 = \rho_2 = 1/2$ and $\sigma^2 = e - v^2$, $2v^4 = 3e^2 - \eta$. Recall that our objective is now to uniquely determine v and $\sigma > 0$ such that $\sigma^2 \leq e$. A necessary and sufficient condition is then clearly $\eta \in (e^2, 3e^2)$. Note that the case $\eta = e^2$ would lead to $\sigma = 0$, meaning that the Gaussian functions degenerate into two Dirac delta functions which correspond to the usual quadrature. The case $\eta = 3e^2$ gives $v = 0$ and both Gaussian functions coincide.

In the case $q \neq 0$, from (2.4), we observe by using the usual algebra of quadrature methods and by setting $\sigma_0 = v_1 v_2$ and $\sigma_1 = -(v_1 + v_2)$, that

$$\left\{ \begin{array}{l} e - \sigma^2 + \sigma_0 = 0, \\ q + \sigma_1 (e - \sigma^2) = 0, \\ \eta - 6\sigma^2 (e - \sigma^2) + 3\sigma^4 + \sigma_1 q + \sigma_0 (e - \sigma^2) = 0. \end{array} \right.$$

The last equation then gives that $\sigma_0 = \sigma^2 - e$ is a root of the third-order polynomial $\mathcal{P}(\sigma_0) = 2\sigma_0^3 + (\eta - 3e^2)\sigma_0 + q^2$. Note that one must have $\sigma_0 \in]-e, 0]$ to fulfill the condition $e \geq \sigma^2$ and to be able to reconstruct $\sigma > 0$ from σ_0. First, since $\lim_{\sigma_0 \to -\infty} = -\infty$, $\mathcal{P}(0) > 0$ and $\mathcal{P}''(\sigma_0) = 12\sigma_0$, there exists a unique root $\sigma_0 < 0$ of $\mathcal{P}$. It then follows that $\sigma_0 > -e$ if and only if $\mathcal{P}(-e) < 0$, that is if and only if $\eta > e^2 + q^2/e$.

2.3. *1-D moment-inversion algorithm*

The three roots of $\mathcal{P}(\sigma_0)$ can be found analytically (one is real, and two are complex conjugates). In the numerical algorithm for moment inversion, the three roots are found from the analytical expressions and the real root is determined by checking the magnitude

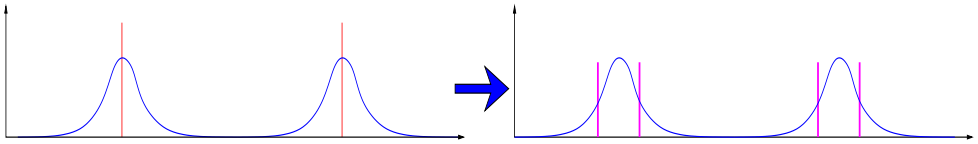

FIGURE 1. Quadrature of the velocity distribution function with a bi-Gaussian distribution (left). Evaluation of a compactly supported distribution, with the same moments up to seventh order as the bi-Gaussian, under the form of a 4-node distribution for flux evaluation.

of the imaginary parts. This method was found to be rapid and robust for all realizable values of e and q. When $M_0 > 0$, the 1-D moment-inversion algorithm then consists of the following three steps:

(a) Given moments $\mathbf{M}$ in Ω, compute e, q and η.

(b) Find real root of $\mathcal{P}(\sigma_0)$, and $\sigma^2 = e + \sigma_0$.

(c) Solve (2.4) according to Desjardins et al. (2008) to find ρ_1, ρ_2, v_1, v_2 (i.e., variables without the overlines). In the case where $\sigma^2 = e$, we set $\rho_2 = v_2 = 0$ and $\rho_1 = M_0$, $v_1 = M_1/M_0$.

When $M_0 = 0$, we set $\rho_1 = \rho_2 = 0$ and (without loss of generality) $\sigma = v_1 = v_2 = 0$.

2.4. *1-D kinetic-based flux algorithm*

The spatial moment fluxes $\mathbf{F}(\mathbf{M})$ are computed using a kinetic-based definition:

$$F_i(t,x) = \int_0^\infty f(t,x,v)v^{i+1}dv + \int_{-\infty}^0 f(t,x,v)v^{i+1}dv, \quad i = 0,\ldots,4; \tag{2.5}$$

where the decomposition into positive and negative directions is used to define the flux function as originally proposed by Bouchut (see de Chaisemartin (2009) and references therein). The numerical representation of the flux function is a critical point in moment transport methods because only *realizable* moment sets can be successfully inverted. We use here an original strategy for the flux evaluation in (Eq. 2.5). We use the presumed form of the distribution f^{G} underlying the quadrature in order to evaluate a higher number of eight moments and eventually use CQMOM in order to generate a compactly supported velocity distribution using a 4-node Gaussian quadrature :

$$f(t,x,v) = \sum\nolimits_{\alpha=1}^{4} \rho_\alpha^*(t,x)\delta\left(v - v_\alpha^*(t,x)\right),$$

which matches the moments up to order seven of the bi-gaussian distribution (and thus the same moments up to order five in system (Eq. 2.1)!) An example of the 4-node quadrature representation is shown in Figure 1. The resulting algorithm for computing the moment fluxes is as follows:

(a) Given moments $\mathbf{M}$, compute ρ_1, ρ_2, v_1, v_2, and σ^2 using the 1-D moment-inversion algorithm in Section 2.3.

(b) Compute $\mathbf{M}^{\mathrm{G}} = (M_0^{\mathrm{G}}, M_1^{\mathrm{G}}, \ldots, M_7^{\mathrm{G}})^t$ from (Eq. 2.2).

(c) Apply the Gaussian quadrature algorithm with $\mathbf{M}^{\mathrm{G}}$ to compute ρ_α^* and v_α^* for $\alpha = 1,\ldots,4$.

(d) Compute spatial moment fluxes using ρ_α^* and v_α^* as described in Vikas et al. (2010).

In order to handle the case where $\sigma^2 = 0$ (i.e., the true distribution is composed of two delta functions), the Gaussian quadrature in step (c) is computed using the adaptive 1-D quadrature algorithm described in Yuan & Fox (2010).

Note that because it is straightforward to compute the moments of f^{G} starting from (Eq. 2.2), the compact representation of the fluxes can be easily extended to include more

than four nodes even if this would rapidly limit the CFL number and increase numerical diffusion. With kinetic-based fluxes, it is possible to derive high-order numerical flux functions that are guaranteed to be realizable when the distribution function is represented by a finite sum of Dirac delta functions (Vikas et al. (2010)). The important point to be underlined here is the fact that we reach the possibility to capture in the fluxes the precise dynamics of two Gaussian distributions and thus differentiate between crossing of two clouds of particles from the dispersion around the mean for each cloud with only five moments effectively transported; in addition it is easy to increase the accuracy of the numerical flux function without increasing the number of transported moments.

3. 2-D kinetic model, multi-Gaussian quadrature, and related algorithms

Defining the bivariate moments

$$M_{i,j}(t,x) = \int_{\mathrm{v}} f(t,x,\mathrm{v}) u^i v^j d\mathrm{v}, \quad i,j = 0,\ldots,N, \quad N \in \mathbb{N},$$

the associated governing equations are easily obtained from (Eq. 1.2):

$$\partial_t M_{i,j} + \partial_x M_{i+1,j} = 0, \quad i,j \geq 0.$$

We will consider in this work a 15-moment model:

$$\left\{\begin{array}{lll} \partial_t M_{0,0} + \partial_x M_{1,0} = 0, & \partial_t M_{0,2} + \partial_x M_{1,2} = 0, & \partial_t M_{4,0} + \partial_x \overline{M}_{5,0} = 0, \\ \partial_t M_{1,0} + \partial_x M_{2,0} = 0, & \partial_t M_{3,0} + \partial_x M_{4,0} = 0, & \partial_t M_{3,1} + \partial_x \overline{M}_{4,1} = 0, \\ \partial_t M_{0,1} + \partial_x M_{1,1} = 0, & \partial_t M_{2,1} + \partial_x M_{3,1} = 0, & \partial_t M_{2,2} + \partial_x \overline{M}_{3,2} = 0, \\ \partial_t M_{2,0} + \partial_x M_{3,0} = 0, & \partial_t M_{1,2} + \partial_x M_{2,2} = 0, & \partial_t M_{1,3} + \partial_x \overline{M}_{2,3} = 0, \\ \partial_t M_{1,1} + \partial_x M_{2,1} = 0, & \partial_t M_{0,3} + \partial_x M_{1,3} = 0, & \partial_t M_{0,4} + \partial_x \overline{M}_{1,4} = 0, \end{array}\right. \tag{3.1}$$

which requires a closure for the fifth-order moments $\overline{M}_{5,0},\ldots,\overline{M}_{1,4}$. We propose to define this closure function by representing f as a multi-Gaussian distribution function. Note that the subset of five bivariate moments with $j = 0$ is the same as those appearing in the 1-D case. Thus, in order for the 2-D closure to be consistent with the 1-D closure, the five moments with $j = 0$ should be treated the same in both closures. A 2-D moment closure with this property will be referred to below as *consistent*.

The 2-D multi-Gaussian distribution function is defined by

$$f^{\mathrm{G}}(\mathrm{v}) = \sum_{\alpha=1}^{4} \frac{\rho_\alpha}{\sqrt{2\pi|\Sigma|}} \exp\left(-\frac{1}{2}(\mathrm{v}-\mathrm{v}_\alpha)^t \Sigma^{-1} (\mathrm{v}-\mathrm{v}_\alpha)\right), \quad \Sigma = \begin{bmatrix} \sigma_{11} & \sigma_{12} \\ \sigma_{12} & \sigma_{22} \end{bmatrix}, \tag{3.2}$$

where Σ is the covariance matrix. In (3.2) there are 15 parameters: $(\rho_\alpha, u_\alpha, v_\alpha, \alpha = 1,\ldots,4)$ and $(\sigma_{11},\sigma_{12},\sigma_{22})$. These parameters must be found by solving the nonlinear system of the form $\mathbf{M} = \mathbf{M}^{\mathrm{G}}$ corresponding to the 15 bivariate moments up to fourth order appearing in (Eq. 3.1). Another advantage of using this form is related to the fact that it naturally includes, as a degenerate case, the non-isotropic joint-Gaussian distribution when the four quadrature nodes coalesce.

In this section we provide a brief description of the 2-D moment inversion algorithm. Before describing the general algorithm, we should note that even in the case where $\Sigma = 0$ (i.e., Dirac delta functions), 2-D moment inversion is non-trivial, see Yuan & Fox (2010). Thus, we cannot expect the moment-inversion algorithm for the multi-Gaussian distribution to be any easier. The algorithm developed in this work makes use of the 2-D conditional quadrature method of moments (CQMOM) described in Yuan & Fox (2010).

Because the kinetic equation in (Eq. 1.2) has non-zero fluxes only in the x direction, it is natural to construct a CQMOM quadrature wherein the v-velocity moments are conditioned on u-velocity. For a 4-node quadrature, the CQMOM algorithm will then use the following subset of ten moments (shown in bold):

$$\begin{bmatrix} \mathbf{M}_{0,0} & \mathbf{M}_{0,1} & \mathbf{M}_{0,2} & \mathbf{M}_{0,3} & M_{0,4} \\ \mathbf{M}_{1,0} & \mathbf{M}_{1,1} & \mathbf{M}_{1,2} & \mathbf{M}_{1,3} & \\ \mathbf{M}_{2,0} & M_{2,1} & M_{2,2} & & \\ \mathbf{M}_{3,0} & M_{3,1} & & & \\ M_{4,0} & & & & \end{bmatrix}.$$

The two moments $M_{2,1}$ and $M_{3,1}$ would be used in CQMOM when the u-velocity moments are conditioned on v-velocity (i.e., when the physical space has two dimensions), and are therefore transported for consistency. As in the 1-D moment-inversion algorithm, $M_{4,0}$ is used to find σ_{11} and $M_{0,4}$ to find σ_{22}. Finally, $M_{2,2}$ is used to find σ_{12}.†

The 2-D moment-inversion algorithm is more complicated than in the 1-D case due to the coupling between the nonlinear equations, and thus will not be described in detail here. However, the basic steps are as follows:

(*a*) Given moments $\mathbf{M}$, compute e_u and q_u.
(*b*) Find real root of $\mathcal{P}(\sigma_0)$, and $\sigma_{11}^2 = e_u + \sigma_0$.
(*c*) Given moments $\mathbf{M}$, compute e_v and q_v.
(*d*) Find real root of $\mathcal{P}(\sigma_0)$, and *initial guess* $\sigma_{22}^2 = e_v + \sigma_0$.
(*e*) Using $\mathbf{M}$, σ_{11}, and σ_{22}, compute σ_{12}.
(*f*) Using CQMOM, construct a 2-D quadrature conditioned on u.
(*g*) Check whether $M_{0,4} = M_{0,4}^{\mathrm{G}}$. If not, update guess for σ_{22} and return to step (*e*) until convergence is achieved.

The iterations are carried out using a bounded secant method. For the example application considered in this work, $\sigma_{12} = 0$ and the unused moments $M_{2,1}$ and $M_{3,1}$ are identically zero. The 2-D moment-inversion algorithm is thus able to recover all 15 transported moments for this example, and hence we can expect that the 2-D moment closure will be consistent.

The spatial moment fluxes are again computed using a kinetic-based definition:

$$F_{i,j} = \int_v \int_0^\infty f(t,x,\mathrm{v}) u^{i+1} v^j du dv + \int_v \int_{-\infty}^0 f(t,x,\mathrm{v}) u^{i+1} v^j du dv,$$

where we approximate f using a 16-node CQMOM quadrature:

$$f(t,x,\mathrm{v}) = \sum_{\alpha=1}^{4} \sum_{\beta=1}^{4} \rho_{\alpha\beta}^*(t,x) \delta\left(u - u_{\alpha\beta}^*(t,x)\right) \delta\left(v - v_{\alpha\beta}^*(t,x)\right)$$

defined using 48 moments found from the multi-Gaussian function in (Eq. 3.2) (see Yuan & Fox (2010) for details). An example of the 16-node quadrature representation is shown in Figure 2. The algorithm for computing the moment fluxes is essentially the same as the one described in Section 2.4 for 1-D quadrature.

† The extension to a 3-D velocity phase space would use the same multi-Gaussian form for f^{G} as in (Eq. 3.2), but with a covariance matrix containing six parameters. The number of additional fourth-order moments in 3-D not used by CQMOM is three, and these are analogous to those used in 2-D for determining Σ (i.e., $M_{0,0,4}$, $M_{2,0,2}$, $M_{0,2,2}$). Thus, it would appear that the multi-Gaussian distribution should also be well defined in 3-D using a 38-moment quadrature.

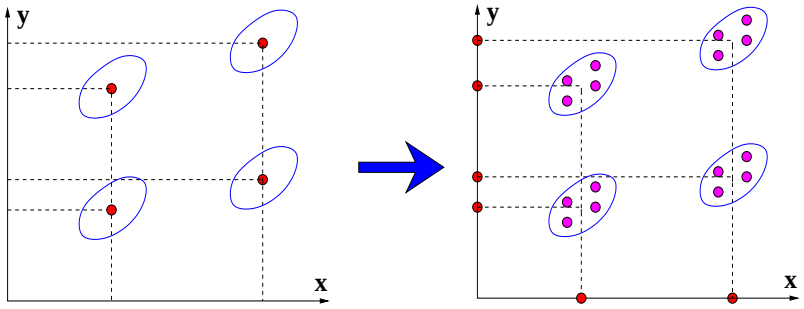

FIGURE 2. Quadrature of the multi-Gaussian velocity distribution function using CQMOM (left) and further evaluation of the flux through a 16-node Dirac delta distribution with the same 48 moments as the multi-Gaussian distribution (right).

4. Riemann problem

As an example application, we will use a Riemann problem with either a 1-D or 2-D velocity phase space. The initial conditions are defined on the real line with a step in the mean u velocity at $x = 0 : U_1 = M_1/M_0 = M_{1,0}/M_{0,0} = \{1, \text{if}\, x < 0, \text{ and } -1, \text{if}\, x > 0\}$. For all x, the initial density is unity and the velocity distribution function is Maxwellian with energy $\sigma^2 = 2/(3(1 + St))$ where St is the particle Stokes number based on the subgrid-scale (SGS) fluid RMS velocity (assumed to be uniform and equal to one), see Reeks (1991). Note that with these initial conditions the velocity distribution is assumed initially to be in equilibrium with the SGS fluid velocity field (i.e., $e_0 = \sigma^2$). However, the discontinuous nature of the mean particle velocity will quickly lead to particle trajectory crossing and a strongly non-equilibrium velocity distribution function.

For 1-D phase space, a measure of the degree of non-equilibrium is the ratio σ^2/e, which is unity for an equilibrium distribution and zero when the distribution is composed entirely of Dirac delta functions. For a 2-D phase space, the ratios σ_{11}/e and σ_{22}/e measure the non-equilibrium behavior in each direction separately. In the Riemann problem described above, the mean v velocity is null so that the velocity distribution should remain in equilibrium in the v direction for all t. In order to identify clearly deviations of the higher-order moments from their equilibrium values, we will use the following normalized moments $e^* = e/e_0$ energy, $q^* = q/e^{3/2}$ skewness, $\eta^* = \eta/e^2$ kurtosis, whose equilibrium values are $e^* = 1$, $q^* = 0$, and $\eta^* = 3$.

In order to solve the moment equations numerically, the 1-D computational domain $-2 < x < 2$ is discretized into 402 finite-volume cells. The spatial fluxes are treated using the first-order kinetic-based approach. The time step is chosen based on the largest magnitude of the abscissas u^*_α used to define the spatial fluxes with a CFL number of 0.5.

5. Results and discussion

Simulation results for the 1-D Riemann problem are presented in Figures 3 and 4 for time $t = 0.5$. Note that due to the equilibrium initial conditions, only one velocity abscissa is used when $\sigma^2/e = 1$ (i.e., v_1) and the other (v_2) is set to zero automatically using the adaptive 1-D quadrature algorithm described in Yuan & Fox (2010). At $t = 0.5$, one can observe that the equilibrium condition is still present on the left and right sides of the computational domain. In the center of the domain, $\sigma^2/e \approx 0.2$, indicating that the overall distribution is composed of two Gaussian distributions with very little overlap.

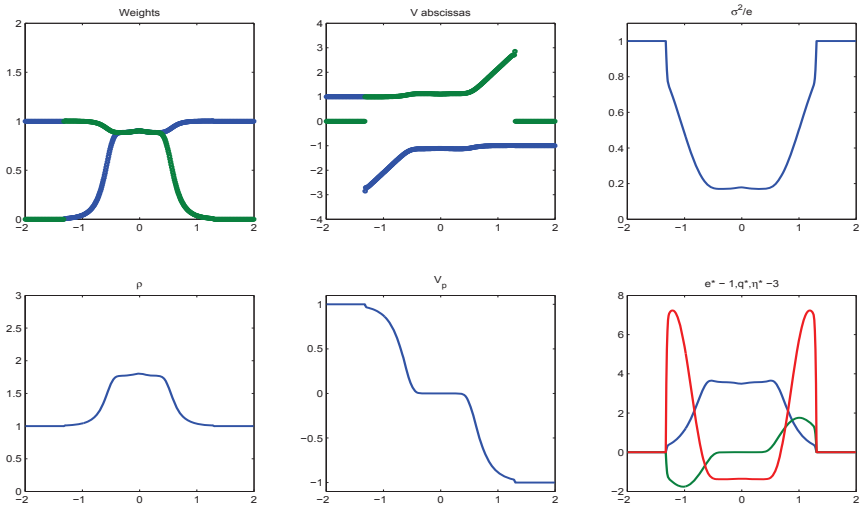

FIGURE 3. Solution to 1-D Riemann problem with $St = 1$ at $t = 0.5$. Top left: Weights ρ_1 (blue), ρ_2 (green). Top center: Abscissas v_1 (blue), v_2 (green). Top right: Gaussian contribution to energy σ^2/e. Bottom left: Density ρ. Bottom center: Mean velocity U_1. Bottom right: Normalized energy $e^* - 1$ (blue), skewness q^* (green), kurtosis $\eta^* - 3$ (red).

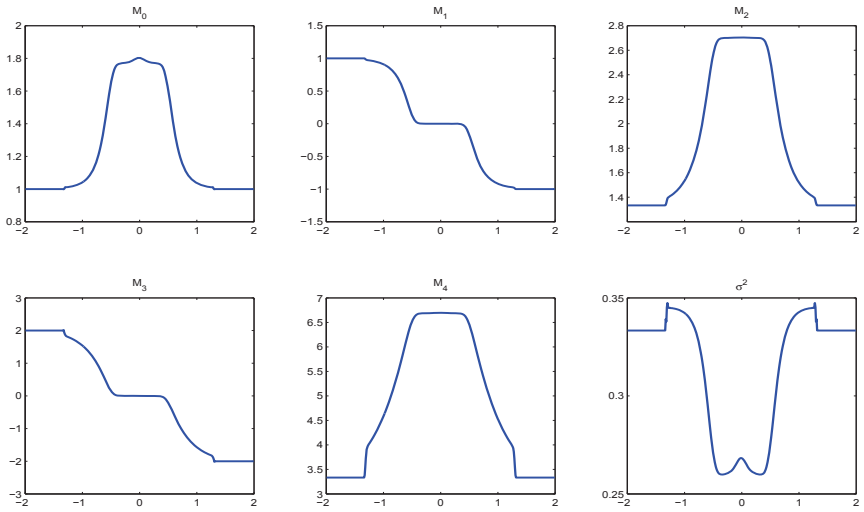

FIGURE 4. Five transported moments and σ^2 for 1-D Riemann problem with $St = 1$ at $t = 0.5$.

Also, note that unlike in a pure PTC problem where the velocity abscissas remain at their initial values (i.e., 1 and -1), in Figure 3 the abscissas have their largest magnitudes just behind the "shock" in density at the edge of the equilibrium domain. This behavior is a direct result of the definition of the spatial fluxes in terms of the underlying bi-Gaussian distribution. Indeed, the outer tails of the Gaussian distribution have higher velocity than the value at the peak density and thus penetrate faster into the equilibrium domain, resulting in a higher local flux velocity. The strong deviations from equilibrium are also clearly observed in the normalized energy, skewness, and kurtosis in Figure 3.

Except at the edges of the equilibrium domain, we see from Figure 4 that the trans-

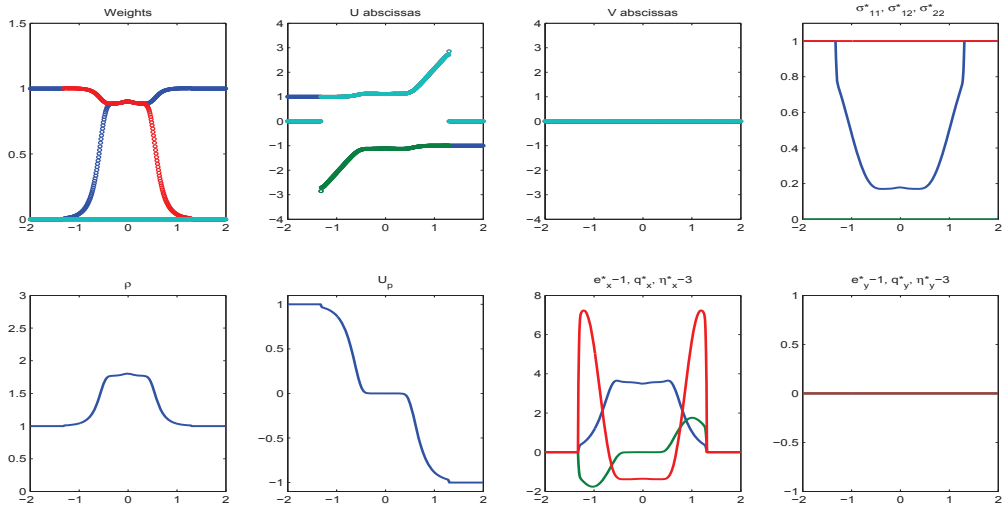

FIGURE 5. Solution to 2-D Riemann problem, $St = 1$ at $t = 0.5$. Top left: Weights ρ_1 (blue), ρ_2 (green), ρ_3 (red), ρ_4 (cyan). Top center-left: u abscissas u_1 (blue), u_2 (green), u_3 (red), u_4 (cyan). Top center-right: v abscissas v_1 (blue), v_2 (green), v_3 (red), v_4 (cyan). Top right: Gaussian contribution to energy σ_{11}/e (blue), σ_{12}/e (green), σ_{22}/e (red). Bottom left: Density ρ. Bottom center-left: Normalized energy $e_u^* - 1$ (blue), skewness q_u^* (green), kurtosis $\eta_u^* - 3$ (red). Bottom right: Normalized energy $e_v^* - 1$ (blue), skewness q_v^* (green), kurtosis $\eta_v^* - 3$ (red).

ported moments and σ^2 are smoothly varying functions of x; more importantly, the singularities appearing in the solution do not belong to the class of δ-shocks but to the less singular class of shocks encountered with hyperbolic systems of conservations laws, thus revealing a potential well-behaved system. Moreover, due to the kinetic-based definition of the spatial fluxes, the moments are always realizable, and the moment-inversion algorithm always computes a well-defined quadrature from the updated moments. Overall, the proposed bi-Gaussian reconstruction of the velocity distribution yields a robust numerical algorithm using a minimum number of moments. In comparison to the high-order delta function reconstruction described in Fox (2009), the bi-Gaussian quadrature provided a higher fidelity flux representation for a fixed number of transported moments. Moreover, because the moments of the bi-Gaussian distribution can be computed to any desired order, the flux representation described in Section 2.4 can be systematically improved without increasing the number of transported moments. This advantage becomes even more significant for 2-D and 3-D phase spaces where the number of transported moments needed for the delta-function reconstruction increases rapidly with the order, see Fox (2009).

Results for the 2-D Riemann problem at $t = 0.4$ are shown in Figures 5 and 6. Comparing first the five moments in Figure 4 to the corresponding moments in Figure 6, we can immediately see that they are identical and thus that the 2-D quadrature algorithm is consistent. Next we can observe that six of the bivariate moments in Figure 6 are null, as is expected from the symmetry of velocity distribution with respect to the v velocity. The moments $M_{0,2}$ and $M_{0,4}$ have the same spatial profile as $M_{0,0}$, which is a result of the v velocity always remaining in equilibrium. This fact can be observed most easily from the plots of the normalized moments in Figure 5. Indeed, only the normalized moments for the u velocity differ from the equilibrium values. Finally, by comparing Figure 3 to the corresponding plots in Figure 5 it is obvious that the 2-D quadrature algorithm agrees

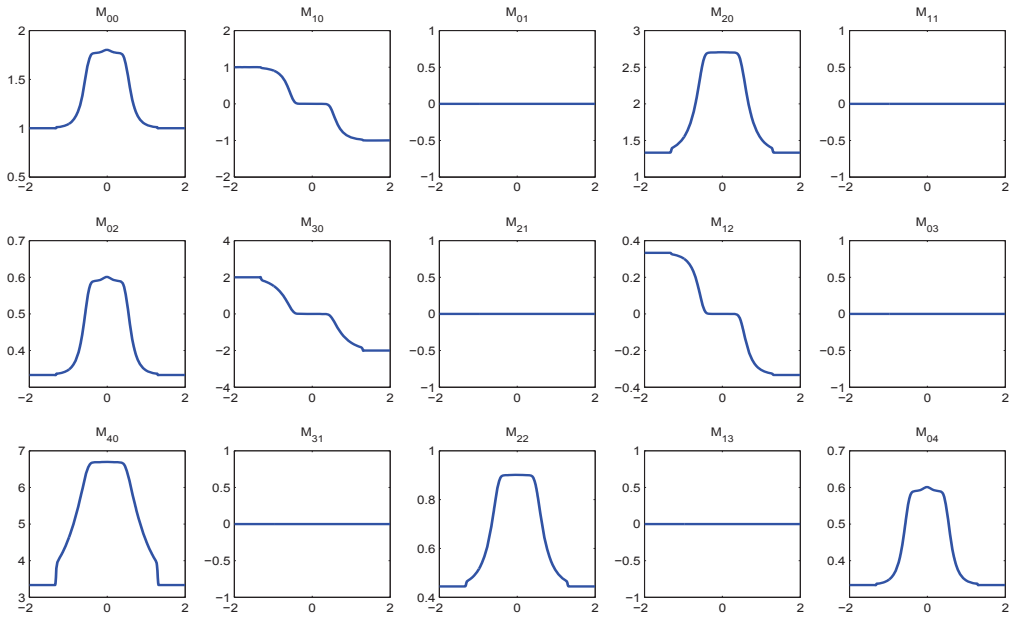

FIGURE 6. Fifteen transported moments for 2-D Riemann problem with $St = 1$ at $t = 0.5$.

exactly with 1-D version. Furthermore, it is especially encouraging to see that the 2-D quadrature can successfully handle degenerate cases where the abscissas coincide without any numerical difficulties (e.g., in the equilibrium region).

6. Conclusions

The proposed quadrature algorithm and related numerical schemes should eventually lead to a very promising solution for solving the filtered NDF for LES of gas-particle flows. The approach combines stability and a lower level of singularity compared to standard quadrature-based moment methods, see Kah et al. (2010), and is able to capture both PTC caused by the free-transport term and the effects of SGS agitation. It is noteworthy that the multi-Gaussian quadrature naturally degenerates toward the correct velocity distribution with the associated spatial fluxes in both the PTC and dispersion limits. Moreover, by relying on the recent advances in CQMOM, see Yuan & Fox (2010), the quadrature naturally adapts to the required number of nodes in even highly degenerate cases (e.g., in the absense of particles).

In order to be generally applicable for approximating solutions to the filtered kinetic equation in complex gas-particle flows, the proposed multi-Gaussian quadrature approach will need to rely on a firmer mathematical background. For example, it will be necessary to prove that it provides a hyperbolic structure (as is suggested by the numerical simulations), and to extend the moment-inversion algorithm to more realistic multi-dimensional configurations. This is the subject of our current research.

Acknowledgments

The authors wish to thank Parviz Moin and the Center for Turbulence Research at Stanford University for their hospitality and financial support.

REFERENCES

Bouchut, F., Jin, S., Li, X. 2003 Numerical approximations of pressureless and isothermal gas dynamics. *SIAM J. Num. Anal.* **41**, 135–158

de Chaisemartin, S. 2009 Polydisperse evaporating spray turbulent dispersion: Eulerian model and numerical simulation. PhD Thesis, Ecole Centrale Paris, available in English at http://tel.archives-ouvertes.fr/tel-00443982/en/

Desjardins, O., Fox, R. O. & Villedieu, P. 2008 A quadrature-based moment method for dilute fluid-particle flows. *J. Comp. Phys.* **227**, 2514–2539.

Fox, R. O. 2009 Higher-order quadrature-based moment methods for kinetic equations. *J. Comp. Phys.* **228**, 7771–7791.

Fréret, L., Thomine, O., Reveillon, J., de Chaisemartin, S., Laurent, F., & Massot, M. 2010 On the role of preferential segregation in flame dynamics in polydisperse evaporating sprays. *Proceedings of the Summer Program 2010, Center for Turbulence Research, Stanford University*, 1–10.

Kah, D., Chalons, C. & Massot, M. 2010 Beyond pressureless gas dynamics: quadrature-based velocity moment models. *Communication in Mathematical Sciences* (submitted)

Kah, D., Laurent, F., Fréret, L., de Chaisemartin, S., Fox, R. O., Reveillon, J. & Massot, M. 2010 Eulerian quadrature-based moment models for dilute polydisperse evaporating sprays. *Flow, Turbulence and Combustion*, online, 1–26.

Reeks, M. W. 1991 On a kinetic equation for the transport of particles in turbulent flows. *Phys. Fluids A* **3**, 446–456.

Vikas, V., Wang, Z. J., Passalacqua, A., & Fox, R. O. 2010 Realizable high-order finite-volume schemes for quadrature-based moment methods. *J. Comp. Phys.* (submitted).

Yuan, C. & Fox, R. O. 2010 Conditional quadrature method of moments for kinetic equations. *J. Comp. Phys.* (submitted).

Zaichik, L. I., Simonin, O., & Alipchenkov, V. M. 2010 An Eulerian approach for large eddy simulation of particle transport in turbulent flows. *J. Turbulence* **10**, 1-21.